# PHYSICS EVALUATION OF COMPACT TOKAMAK IGNITION EXPERIMENTS*

CONF-851102--49

DE86 003806



N. A. Uckan, W. A. Houlberg, and J. Sheffield
Oak Ridge National Laboratory
Oak Ridge, Tennessee 37831

Abstract: At present, several approaches for compact, high-field tokamak ignition experiments are being considered. A comprehensive method for analyzing the potential physics operating regimes and plasma performance characteristics of such ignition experiments with 0-D (analytic) and 1-1/2-D (WHIST) transport models is presented. The results from both calculations are in agreement and show that there are regimes in parameter space in which a class of small ($R_o$ ~ 1-2 m), high-field ($B_o$ ~ 8-13 T) tokamaks with $aB_o^2/q_* \sim 25 \pm 5$ and $\kappa = b/a \sim 1.6$-2.0 appears ignitable for a reasonable range of transport assumptions. Considering both the density and beta limits, an evaluation of the performance is presented for various forms of $\chi_e$ and $\chi_i$, including degradation at high power and sawtooth activity. The prospects of ohmic ignition are also examined.

## 1. Introduction

The physics of ignition is one of the key areas that remain to be addressed by the magnetic fusion research program. It is expected that the next phase of this program will involve a compact ($R_o$ ~ 1-2 m), high-field ($B_o$ ~ 8-13 T) tokamak with the goal of providing an ignited plasma for pulses of several seconds ($\tau_{pulse} \simeq 10\tau_E$) to study the properties of burning plasmas.[1] In this paper, we present a comprehensive method for analyzing the potential physics operating regimes and plasma performance characteristics of such ignition experiments using both the global analytic model[2] and the POPCON (Plasma OPeration CONtour) analysis of the 1-1/2-D WHIST transport code.[3] Details of both models are described elsewhere[2,3] and briefly summarized here.

First, the global model is used to establish the physics requirements and options for ignited plasmas. For a given set of physics assumptions ($\chi_e$ and $\chi_i$ or $\tau_E$, $\beta_{crit}$, $n_{max}$, $q_\psi$, etc.), steady-state plasma performance contours are generated for analysis of a particular device or a class of devices with equivalent performance. These contour plots are used to show the relationship between driven and ignited operation; the prospect of achieving ignition with ohmic heating alone; the optimal path to ignition; and the sensitivity to variations in confinement models ($\chi$'s or $\tau$'s), mild plasma shaping ($\kappa \sim b/a$), and sawtooth activity [modeled through the on-axis safety factor q(0) in global analysis].

The 1-1/2-D WHIST transport code is then used to obtain POPCON plots for a few selected reference ignition experiments and to model/examine the physics issues critical to attainment of ignition (such as alpha particle physics, sawtooth oscillations, and confinement degradation with heating power). Plasma performance contours (POPCONs) obtained from the global and the 1-1/2-D models are found to be in reasonable agreement, showing similar features and trends as well as comparable magnitudes. The WHIST results, especially those with dynamic startup simulations and sawtooth modeling (in which poloidal magnetic energy is converted into kinetic energy during a sawtooth crash), are slightly more favorable, signifying the importance of profile evolution and nonlinear, spatially localized physical processes.

*Research sponsored by the Office of Fusion Energy, U.S. Department of Energy, under Contract No. DE-AC05-840R21400 with Martin Marietta Energy System, Inc.

In the analysis presented here, an attempt has been made to cover the range of possibilities for the confinement scalings (optimistic, ohmic-like scaling to pessimistic, L-mode-like scaling), thus bracketing the options for ignition experiments. Results obtained may provide a useful guidance for future design improvements and/or selections.

In all expressions, unless otherwise stated, the average values for density (<n>), density-averaged temperature (<T> = <nT>/<n>), etc., are used (without the angle brackets). The units are mks, with T in keV, current I in MA, and power in MW. When designated, $n_{20} = n/10^{20} m^{-3}$ and $T_{10} = T/10$ keV.

## 2. Models

In recent years, 1-1/2-D (1-D transport coupled with 2-D MHD equilibrium), time-dependent transport simulations and POPCON analysis with the WHIST code have been routinely used to evaluate the performance of various fusion reactors and/or experiments.[3] An analytic model[2] has recently been developed that complements the full 1-1/2-D code calculation and expands its POPCON capability in some areas: it allows not only rapid assessment of the ignition requirements and plasma operating regimes of a particular device, but also formulation of nearly universal POPCON plots for classes of devices with equivalent performance.

To obtain the global power balance equations, the flux-surface-averaged particle and energy balance equations of the 1-1/2-D model are volume-averaged over model plasma profiles, which are determined from the principle of profile consistency.[4] The global model ignores the edge region and is not suitable (by definition) for predicting the sawtooth activity, other than simply parameterizing it in terms of the on-axis safety factor $q(0) \leq 1$ and $r_s$, the radius of the $q = 1$ surface. Experimental observations[5,6] from ohmic and auxiliary heated plasmas, however, appear to indicate that the central sawtooth region plays a minor role in the overall energy balance and that natural profiles exist for $T_e(r)$ and $q(r)$, associated with the safety factor at the edge $q_*(a)$, where $q_*$ is the equivalent cylindrical safety factor. Thus, consideration of consistent profiles with q(0) as a parameter should provide reasonable global plasma performance predictions. Although good confinement characteristics of the sawtooth region do not appear to play a role in the overall energy balance, its behavior is of great importance for the compact ignition experiments in which ignition may well be possible in the central region during a sawtooth rise. Details of these characteristics are discussed in Ref. 7.

Other features included in the global model are:[2] neoclassical enhancement of resistivity ($\bar{\gamma}_{NC}$); various forms of ion ($\chi_i$) and electron ($\chi_e$) thermal diffusivities or global energy confinement times ($\tau_E$); fast-alpha contribution to total pressure; fuel, alpha, and impurities ($Z_{eff}$); and various constraints imposed by equilibrium, stability, and confinement ($q_\psi$, $\beta_{crit}$, $n_{max}$, etc.). Some of these constraints are described below.

The density is limited by the Murakami limit,[8] taken as

$$n_{e20} < n_{mu} \simeq 1.5\, B_o/q_* R_o \,.$$

The maximum volume-averaged beta is limited by the Troyon limit,[9] taken as

$$\beta < \beta_{crit} \simeq 3 \times 10^{-2}\ I/aB_o\ , \qquad (2)$$

where $\beta = \beta_e + \beta_i + \beta_{f\alpha} = (1 + \gamma_{f\alpha})(\beta_e + \beta_i)$, with $\gamma_{f\alpha}$ the ratio of the fast-alpha pressure to the plasma thermal pressure (typically $\gamma_{f\alpha} \sim 5$-$25\%$ for T ~ 6-16 keV). The relationship between plasma current I, magnetic field $B_o$, true MHD safety factor $q_\psi$, and plasma shape ($\kappa$, $\delta \leq 0.4$, $\varepsilon = a/R_o$) is

$$I = \frac{5aB_o}{q_\psi}\frac{a}{R_o}\left[\frac{1 + \kappa^2(1 + 2\delta^2)}{2}\right] f(\varepsilon)$$

$$= \frac{5a^2B_o}{q_* R_o}\left[\frac{1 + \kappa^2(1 + 2\delta^2)}{2}\right] , \qquad (3)$$

where $q_\psi = f(\varepsilon)q_*$ with $f(\varepsilon) \simeq (1.22 - 0.68\varepsilon)/(1 - \varepsilon^2)^2$.

Transport assumptions include neoclassical (Chang-Hinton[10]) losses for all thermal ion species (of common temperature $T_i$), $\chi_i = f_{ix}\chi_{CH}$, with $f_{ix} \sim 1$-3. The scaling laws for $\chi_e$ or $\tau_{Ee}$ (or $\tau_E$) are empirical and numerous. In an attempt to cover the range of possibilities and to bracket the answers, we choose two examples[6,11] that represent ohmic ($\tau_{EOH}$) and auxiliary ($\tau_{Eaux}$) scalings, respectively.

1. Neo-Alcator scaling ($\tau_E$ or $\tau_{Ee}$):

$$\tau_{NA} = 0.07 n_{e20} a R_o^2 q_* \ ; \quad \chi_{NA} \simeq \frac{4.3a}{n_{e20} R_o^2 q_*}\left(\frac{2\kappa^2}{1 + \kappa^2}\right) g(r) \ . \qquad (4)$$

2. Kaye-Goldston scaling (L- and H-mode):

$$\tau_{EKG}^L \simeq 0.056 I^{1.24} P^{-0.58} R^{1.65} a^{-0.49} \kappa^{0.28} n_{e20}^{0.26} B_\phi^{-0.09} A_i^{0.5} ,$$

$$\chi_{KG} \simeq (0.3a^2/\tau_{EKG})[2\kappa^2/(1 + \kappa^2)] g(r) \ , \qquad (5)$$

where $g(r) = [1 + 4(r/a)^2]/2$ is the radial shape factor in the WHIST code [$g(r) = 1$ in global calculations], $A_i$ = ion atomic mass number (which is added to the original scaling to include the isotope effect on confinement, as seen by various experiments), and P = heating (ohmic + alpha + auxiliary - radiation) power ~ $\langle nT/\tau_E \rangle$. Typically, $\tau_E$(H-mode) ≃ $2\tau_E$(L-mode). In the 1-1/2-D calculations, $\chi_e \simeq 0.8(\chi_{NA}$ or $\chi_{KG})$, $\chi_i = 0.2\chi_e + f_{ix}\chi_{CH}$, and the particle diffusion coefficient is taken as $D = 0.2\chi_e$.

The first example (neo-Alcator scaling) has been chosen because of its wide use in low-density ohmic plasmas. However, in high-density ohmic plasmas, $\tau_E$ does not scale linearly with density, showing scaling characteristics similar to those observed in L-mode (poor confinement) auxiliary heated plasmas. In general, a typical L-mode scaling has the form

$$\tau_E^L \sim I^{(1 \text{ to } 1.5)}\left[P^{-(1/3 \text{ to } 2/3)} \text{ or } C_1 + C_2/P\right] \ ; \qquad (6)$$

Eq. (5) is one example of this type. A generalized ohmic/auxiliary scaling is defined as[12,13]

$$\tau_E = \left(\tau_{EOH}^{-2} + \tau_{Eaux}^{-2}\right)^{-1/2} \ , \qquad (7)$$

and fits data from ohmic and auxiliary heated plasmas.

We note that, while we use these "empirical" scalings to establish ignition conditions and determine range of expected plasma performance characteristics of a given device and/or class of devices, the results presented should be viewed as relative trends, because the confinement properties of burning plasmas may or may not obey the empirical scaling laws selected. Nonetheless, the analyses presented here satisfy the need to compare relative merits and potentials of devices with different parameters and to identify those operating regimes and/or classes of devices with similar (different) characteristics.

The global power balance equation, combined for electrons and ions, written in symbolic form, is

$$F = \frac{\partial W}{\partial t} = -P_{con} - P_{rad} + P_\alpha + P_{OH} + P_{aux} \ , \qquad (8)$$

where W is the total plasma energy density and the terms on the right side represent the power loss due to transport processes ($P_{con} = P_e + P_i$), the bremsstrahlung radiation ($P_{rad}$), the alpha power ($P_\alpha$), the ohmic power ($P_{OH}$), and the auxiliary power ($P_{aux}$). Detailed explicit expressions are given in Ref. 2; a simplified form is given in the appendix.

Because of the high density and relatively low ignition temperatures of the compact ignition experiments, the thermalization term ($Q_{ei}$) is very strong and $T_e \simeq T_i$. This permits a single-fluid treatment and makes analyses using a global $\tau_E$ more reliable because over the entire range $f_{nT} = n_iT_i/n_eT_e \sim n_i/n_e$, which is nearly constant. In low-density experiments, the separation between electron and ion confinement is more critical because decoupling may occur and "hot ion mode" behavior may result if $\tau_{Ei} \gg \tau_{Ee}$. In those cases $f_{nT}$ may increase strongly with temperature, requiring two-fluid treatment.

A typical set of steady-state plasma parameter curves in density/temperature space is shown in Fig. 1. Shown are ohmic (OH) equilibrium and ignition contours ($P_{aux} = 0$), the thermal runaway contour ($\partial P_{aux}/\partial T = 0$), and the limits imposed by the Murakami density limit and the Troyon beta limit. The heating window [$P_{aux} > 0$, $(\Delta T)_h = T_{IGN} - T_{OH}$] and operating window [$(\Delta T)_{op}$; $(\Delta n)_{op}$ -- dotted region] are indicated. The optimal path to ignition is where $(\Delta T)_h$ (and $P_{aux}$) is minimum (narrowest heating window). If $(\Delta T)_h = 0$, ohmic ignition is accessible. If, on the other hand, $(\Delta T)_{op}$ [or $(\Delta n)_{op}$] = 0, the beta limit (or density limit) is reached before ignition is achieved. For ignition experiments, the existence of a large $(\Delta T)_{op}$ [and $(\Delta n)_{op}$] is important because it permits separation of physics of ignition and burning plasma properties from those associated with beta and density limits. The size of this operating window is a measure of the ignition margin $M_I$, which is defined as

$$M_I = (P_\alpha + P_{OH})/(P_{rad} + P_{con}) \ . \qquad (9)$$

$M_I = 1$ gives the ignition condition, which corresponds to a "point" operating window where all three curves (ignition contour and beta and density limits) meet.

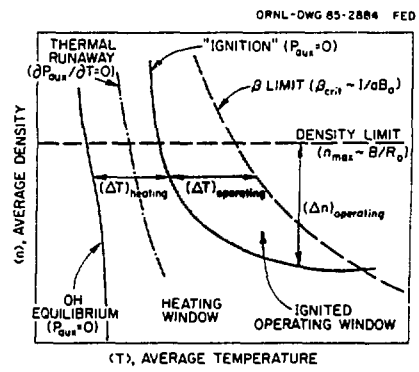


Fig. 1. Typical plasma parameter operating space.

## 3. Generalized Contour Analysis of Ignition Conditions

The global power balance equation [Eq. (A-5)], subject to a given set of physics models and constraints, could be used to determine the options for an ignition experiment. Classes of devices with equivalent performance could also be identified if the problem can be formulated in terms of a small number of parameters. For the range of confinement scalings considered ($\chi_i \sim \chi_{CH}$ and $\chi_e \sim \chi_{NA}, \chi_{KG}$ or $\tau_E \sim \tau_{NA}, \tau_{KG}$), such a formulation is shown to be possible in terms of the Murakami density limit ($m = n_{e20}/n_{mu}$), temperature ($T$), and $aB_o^2/q_*$, the "figure-of-merit" parameter. Similar parameterization (in terms of these or any other similar quantities) is also possible for other confinement scalings.

The confinement scalings selected here cover the range of possibilities ("optimistic" ohmic scaling, such as neo-Alcator, and "pessimistic" L-mode auxiliary scaling, such as Kaye-Goldston), thus providing useful guidance (lower and upper bounds) on the options for ignition devices. Eventual selection of one of these options as an "optimum" depends on other criteria and constraints imposed by engineering, technology, and cost considerations. Additional physics considerations, such as startup, flattop time, and volt-second requirements (as discussed in Ref. 7), could also influence the selection process.

For high-field, compact ignition experiments, a typical parameter range considered is $R_o \sim 1$-$2$ m, $B \sim 8$-$13$ T, $A \sim 3 \pm 0.5$, $q_\psi \sim 2.6$ ($q_* \sim 2$), and $Z_{eff} \sim 1.5$. For a "standard" tokamak, $\kappa \sim 1.6$-$1.7$ and $\delta \sim 0$-$0.2$. Increased elongation ($\kappa \sim 2$) could, however, improve both the beta limit ($\beta \sim I/aB_o$) and $\tau_{KG}$ ($\sim I^{2.95}$).

### 3.1 Ohmic Scaling

First we consider neo-Alcator-like ohmic scaling ($\tau \sim naR^2q_*$) because of its wide use in various fusion reactor design studies and in initial compact ignition design studies.[14-16] Scaling of this kind ($\tau \sim n$) describes only low-density ohmic plasmas. At high densities, a partial ($\tau \sim n^x$, $x < 1$) or complete ($\tau \sim n^0$) saturation occurs, though it may be possible to extend the density range where $\tau \sim n$ with pellet fueling. The use of auxiliary heating further degrades the confinement. The results obtained with the neo-Alcator scaling should therefore provide the optimistic limit.

Taking $\chi_e = f_{ex}\chi_{NA}$ and $\chi_i = f_{ix}\chi_{CH}$ with $f_{ex} \sim 1$-$2$ and $f_{ix} \sim 1$-$3$, the ignition condition is

$$-a_e T_{10} - (a_i + a_B)m^2 T_{10}^{1/2} + a_\alpha m^2 T_{10}^{S} + a_{OH} T_{10}^{-3/2} = 0 \quad , \tag{10}$$

where $a_B$, $a_\alpha$, and $a_{OH}$ are given in Eq. (A-7), and

$$a_e \simeq 3.43 f_{ex}/(aB_o^2/q_*) \quad , \tag{11a}$$

$$a_i \simeq 0.7 f_{ix}(Z_{eff}/1.5)(1.6/\kappa)^2/(aB_o^2/q_*) \quad . \tag{11b}$$

In Eq. (11b) we assumed $A \sim 3 \pm 0.5$ and $q_\psi \sim 2.6$.

Equation (10) can be solved analytically [$m = f(T)$] for a given value of $aB_o^2/q_*$, and the solution is nearly independent of any other parameter for the range of standard tokamak parameters given earlier. In Fig. 2, ignition (OH equilibrium) contours for various values of $aB_o^2/q_*$ are plotted in ($m = \langle n \rangle / n_{mu}$, $\langle T \rangle$) space for $f_{ex} = 1$, $f_{ix} = 1$ and 3, and $q(0) = 0.8$ and 1.0. The $\beta = \beta_{crit}$ contours are superimposed (note that within the parameter range of interest, $aB_o \sim 4.5$-$5.0$).[2] The contribution from fast alphas is included in the total pressure.[2] For a given $aB_o^2/q_*$, $P_{aux} = 0$ on the designated curves. The following information can readily be obtained from Fig. 2: (i) relative size of heating and operating windows (and their variation with $aB_o^2/q_*$), (ii) the optimal path to ignition, (iii) requirements for ohmic ignition, and (iv) the effect of assumption of $q(0) = 1.0$ or 0.8. We note that when electron losses are doubled, $f_{ex} = 2.0$, the devices with $aB_o^2/q_* < 20$ reach their density and beta limits before they achieve ignition.

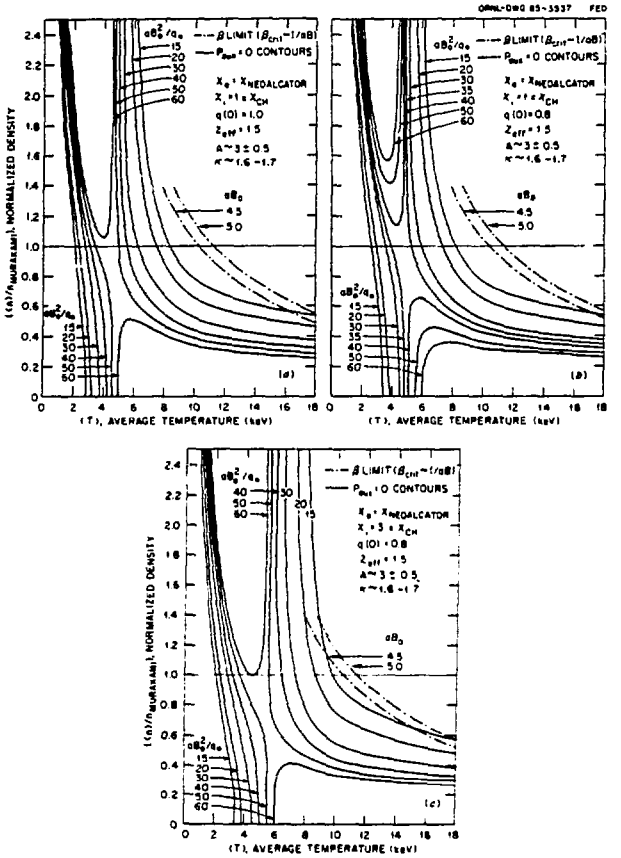


Fig. 2. Steady-state ignition (OH equilibrium) contours for ohmic-like scalings for various values of $aB_o^2/q_*$. $\beta = \beta_{crit}$ contours (including fast-$\alpha$ pressure) are superimposed. [Confinement model, $q(0)$, and selected geometry are indicated.] For $m \lesssim 1$, ohmic ignition is possible if (a) $aB_o^2/q_* > 52$, (b) $aB_o^2/q_* > 37$, and (c) $aB_o^2/q_* > 55$.

Increased plasma elongation ($\kappa \sim 2$) does not alter the ignition contours much (<10%), but it does improve the beta limit (~30%) through an increase in plasma current for a given $q_\psi$ ($q_*$), thus enlarging the operating window (and increasing the ignition margin). A simple picture of this effect can be seen by a nearly parallel slide of $\beta = \beta_{crit}$ contours in Fig. 2 (by about 25-30%) to higher temperatures, though the fast-alpha contribution to beta alters this simple picture somewhat.

### 3.2 Ohmic + Auxiliary Scaling

Next we consider the more pessimistic predictions of a Kaye-Goldston-like L-(H-)mode scaling ($\tau \sim P^{-\alpha}$ with $\alpha \sim 1/3$-$1/2$; $P_\alpha$ and $P_{OH}$ are included in P, in addition to $P_{aux}$). A generalized form of ohmic/auxiliary scaling is given by Eq. (7). Taking $\tau_{EOH} = \tau_{NA}$ and $\tau_{Eaux} = f_{KG}\tau_{EKG}^L$, where $f_{KG} = 1$ (2) for L-(H-)mode, the ignition requirement is

$$-T_{10}\left(a_{EOH}^2 + a_{KG}^2 m^{3.5} T_{10}^{2.76}\right)^{1/2} - a_B m^2 T_{10}^{1/2} + a_\alpha m^2 T_{10}^S + a_{OH} T_{10}^{-3/2} = 0 \qquad (12)$$

where

$$a_{EOH} = (1 + f_{nT})a_e = 6.52/(aB_o^2/q_*) \quad ,$$

$$a_{KG} \propto \frac{50}{(aB_o^2/q_*)^{1.5}} \left[\frac{a^{0.2} q_*^{1.7}}{(a/R_o)^{0.65}}\right] \frac{\kappa^{0.7}}{f_{KG}} \left(\frac{2}{1+\kappa_*^2}\right)^{2.95} . \qquad (13)$$

For a typical range of parameters, the term in square brackets in Eq. (13) is nearly constant and is roughly $5.5 \pm 0.3$ for $A = R_o/a \sim 2.8 \pm 0.2$ (for $A \sim 3 \pm 0.5$, it has a value of $\sim 5.8 \pm 0.7$). Thus the dependence of $a_{KG}$ on the terms in brackets can be neglected. There is a strong dependence on plasma shape.

To illustrate the effect of plasma shaping, we consider three geometries with increasing elongation:

I. $\kappa \sim 1.6\text{-}1.7$, $\delta \sim 0.3\text{-}0.1$,
II. $\kappa \sim 1.9\text{-}2.1$, $\delta \sim 0.2\text{-}0.0$,
III. $\kappa \sim 2.3\text{-}2.5$, $\delta \sim 0.2\text{-}0.0$.

In all cases $A \sim 2.8 \pm 0.2$ and $q_\psi \sim 2.6$ ($q_* \sim 2$). Note that, for a given $aB_o^2/q_*$, the plasma current is higher by about a factor 1.3 and $(1.3)^2$ in geometries II and III, respectively, than in geometry I.

The following observations can be readily obtained from Eq. (12). For a given $aB_o^2/q_*$, the ignition contour of (1) I (H-mode, $f_{KG} = 2$) is about the same as II (L-mode, $f_{KG} = 1$), and (2) I ("super" H-mode, $f_{KG} = 4$) is about the same as II (H-mode), which is about the same as III (L-mode). The beta limits, however, are larger in III than in II and larger in II than in I by an amount proportional to their current ratios.

Figure 3 summarizes these observations. Shown are ignition contours for various values of $aB_o^2/q_*$ for the geometries (I, II, III) considered. Corresponding beta contours are also superimposed. An L-mode scaling places very stringent requirements on a standard tokamak (geometry I); devices with $aB_o^2/q_* < 27$ reach their beta and density limit before ignition is achieved (Fig. 3a). The possibility of an H-mode and/or some increased elongation (Fig. 3b) relieves some of this problem (now ignition appears to be possible for $aB_o^2/q_* > 20$). Still further increase in elongation (geometry III) reduces this limit to about 15. We note that these findings [that whether the plasma shaping (large $\kappa$) really helps to improve confinement (as well as beta limit)] are subject to experimental verification. This is because the experimental data from which these scalings are deduced are typically limited to a range at which $\kappa < 1.6$.

Comparison of Figs. 2 and 3 indicates the effect of confinement degradation with total heating (ohmic + alpha + auxiliary) power. Although the effect is uniform, the impact on devices with $aB_o^2/q_* < 30$ for a standard tokamak (geometry I) and $< 20$ for an elongated tokamak (geometry II) is more pronounced.

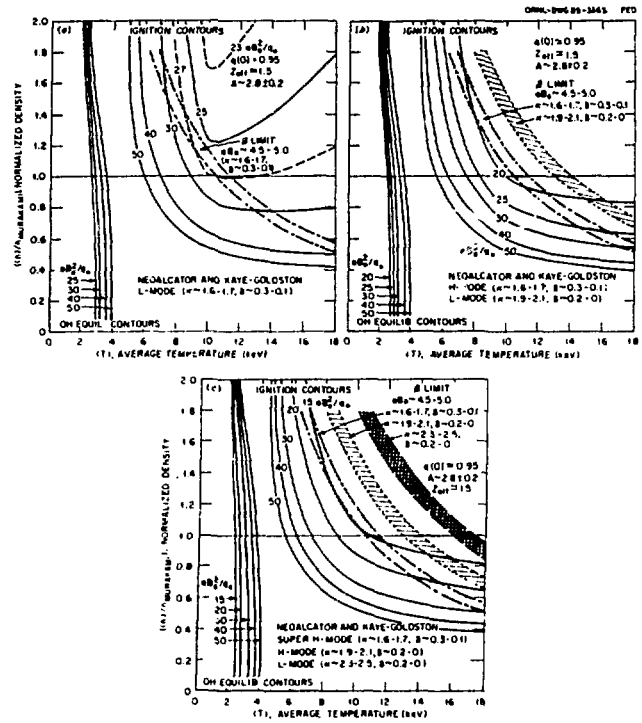


Fig. 3. Steady-state ignition contours for various values of $aB_o^2/q_*$ for neo-Alcator and Kaye-Goldston (L-, H-mode) scalings in three different geometries (as defined in the text and shown in the figure). $\beta = \beta_{crit}$ contours corresponding to each geometry are superimposed.

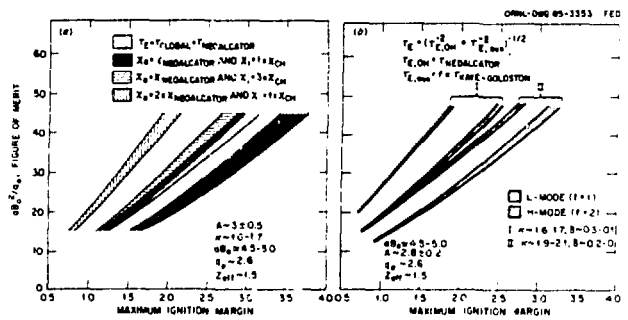


Fig. 4. Maximum attainable ignition margin vs $aB_o^2/q_*$ for (a) ohmic-like and (b) ohmic + auxiliary scalings.

## 3.3 Margin for Ignition

The ignition margin is defined by Eq. (9). The maximum margin for ignition within the plasma operating window is obtained where $n = n_{mu}$ ($m = 1$), and $\beta = \beta_{crit}$ if the confinement scaling is of the form $\tau \sim n^x T^y$, with $x > y$ and $\langle\sigma v\rangle \sim T^2$. Figure 4 shows the maximum attainable ignition margin vs $aB_o^2/q_*$ for the range of confinement scalings and tokamak geometries considered earlier.

## 4. Plasma Performance Analysis: 0-D and 1-1/2-D

The performance of representative high-field, compact ignition devices[14-16] is examined using both the global equations and the 1-1/2-D WHIST code. Representative machine parameters under consideration are summarized in Table 1. In principle these can be grouped as

1. devices with $aB_o^2/q_* \sim 20$ and
2. devices with $aB_o^2/q_* \sim 30\text{-}32$.

Although designs are evolving and parameters are changing, examples from these two groups are used for purposes of illustration.

For a typical range of aspect ratios ($A \sim 2.5\text{-}3.0$) and $q_\psi \sim 2.6$, the range of device parameters corresponding to $aB_o^2/q_* \sim 20\text{-}35$ is plotted in Fig. 5. The corresponding plasma current I is ~7-10 MA for a standard (I) tokamak, ~9-13 MA for elongated (II)

Table 1. Typical parameters[a,b,c]

| | IGNITOR-A[a] | PPPL-ISP[b] (0424) | MIT-LITE[c] |
|---|---|---|---|
| $R_0$(m) | 1.01 | 1.62 | 1.76 |
| a(m) | 0.39 | 0.53 | 0.55 |
| $A = R_0/a$ | 2.6 | 3.0 | 3.2 |
| $\kappa$ (-) | 1.67 | 1.6 | 1.6 |
| $\delta$ (-) | 0.25 | 0.4 | 0.3 |
| $B_0$(T) | 12.6 | 9.0 | 8.6 |
| I(MA) | 10.0 | 8.0 | 7.0 |
| $q_\psi$ (-) | 2.6 | 2.6 | 2.6 |

a,b,c,At present the following variations are also being considered.

[a]larger $R_0$; lower $B_0$; similar A, $\kappa$.

[b]higher $B_0$, I, $\kappa$; similar A.

[c]higher $B_0$ but smaller $R_0$ I, and $\kappa$; larger A.

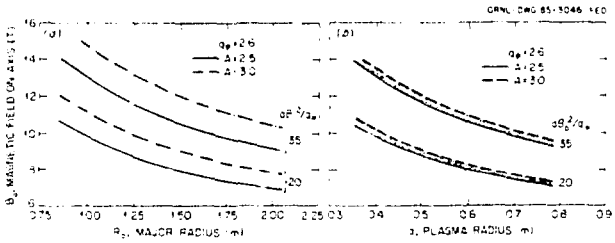

Fig. 5. Range of device parameters ($B_0$, $R_0$, a) corresponding to $aB_0^2/q_* \sim 20$-35 for A ~ 2.5-3.0 and $q_\psi \sim 2.6$.

tokamak, and ~12-17 MA in geometry III. For most parameters, the range of interest is $aB_0 \sim 4.5$-5.0 (Fig. 5).

Standard parameters and geometry (I) assumed for the contour plots in Figs. 2 and 3 are representative (within 10-15%) of the ignition experiments listed in Table 1; thus, any results given are directly applicable.

### 4.1 Devices with $aB_0^2/q_* \sim 20$

This class of devices is representative of early versions of MIT-LITE[16] and PPPL-ISP.[15] Steady-state auxiliary power contours and critical beta contours showing ignition (and OH equilibrium), relative size of heating and operating windows, and optimal density path are plotted in Fig. 6 for ohmic-like scalings and in Fig. 7 for ohmic + auxiliary scalings, both of which are calculated analytically. In a standard (I) tokamak geometry ($\kappa \sim 1.6$-1.7), although ignition appears possible with a reasonable margin (requiring $P_{aux} \sim$ 5-10 MW of steady-state absorbed power) for neo-Alcator-like ohmic scalings (Fig. 6a,b), ignition is not accessible (even in the absence of beta and density limits) for an L-mode Kaye-Goldston scaling (Fig. 7a). Figure 7a also shows Q-contours, where $Q = P_{fus}/(P_{aux} + P_{OH}) \sim P_{fus}/P_{aux}$, that indicate a reasonable operating window for $Q > 5(<10)$ requiring $P_{aux} \gtrsim 25$ MW. The possibility of an H-mode operation and/or plasma shaping (Fig. 7b) appears to alleviate the problem somewhat. The resulting operating window in this case is finite but small.

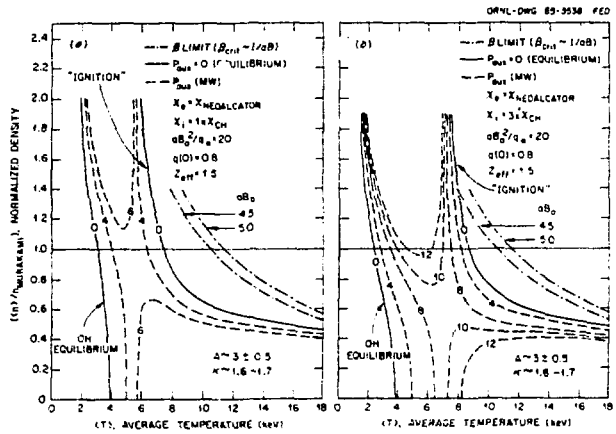

Fig. 6. Steady-state auxiliary power contours and critical beta contours for classes of devices with $aB_0^2/q_* = 20$ for ohmic-like scalings.

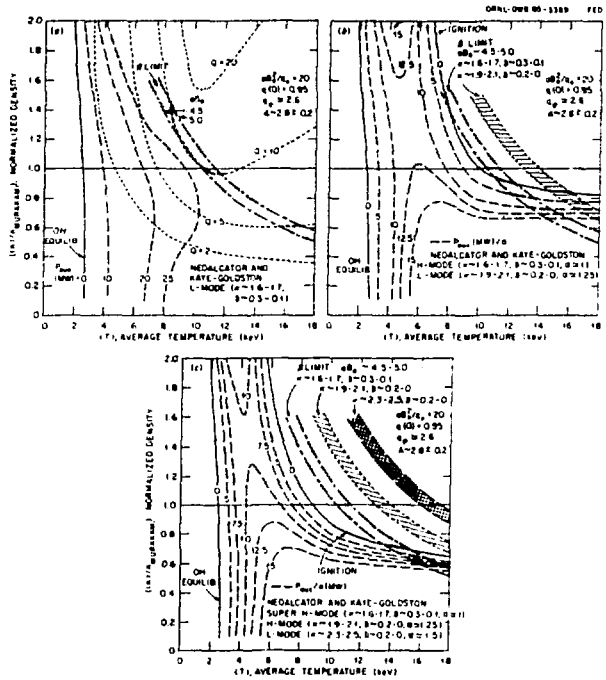

Fig. 7. Same as Fig. 6 except the confinement model is ohmic + auxiliary scaling (neo-Alcator and Kaye-Goldston) for L- and H-modes in different geometries. $Q = P_{fus}/(P_{aux} + P_{OH})$ contours are superimposed (a).

POPCON plots (1-1/2-D results) for auxiliary power, Q, and critical beta are given in Fig. 8 both for (a) ohmic and (b) L-mode scalings. Comparison of results (analytic vs 1-1/2-D) from Figs. 8a and 6a and 8b and 7a indicates similar characteristics and shows a reasonable agreement. Contours of the total fusion power output and the average toroidal and poloidal beta are shown in Fig. 9.

### 4.2 Devices with $aB_0^2/q_* \sim 32$

This class of devices is representative of Ignitor-A.[14] Steady-state auxiliary power contours, similar to those in Figs. 6-7, are given in

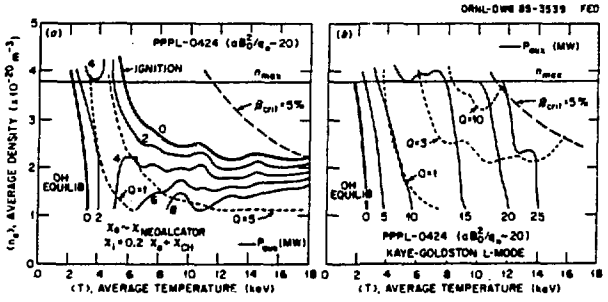


Fig. 8. Steady-state POPCON plots showing auxiliary power ($P_{aux}$) and Q contours for a typical ignition device with $aB_0^2/q_* \sim 20$ (PPPL-ISP device parameters given in Table 1 are used). $n = n_{max}$ ($\sim 3.9 \times 10^{20}$ m$^{-3}$) and $\beta = \beta_{crit}$ (~5%) are shown. Confinement models (a) ohmic (neo-Alcator) scaling and (b) generalized neo-Alcator and Kaye-Goldston scaling (L-mode). The fluctuations in the $P_{aux}$ contours reflect the effects of discrete sawtooth activity even though some smoothing of the data has been done.

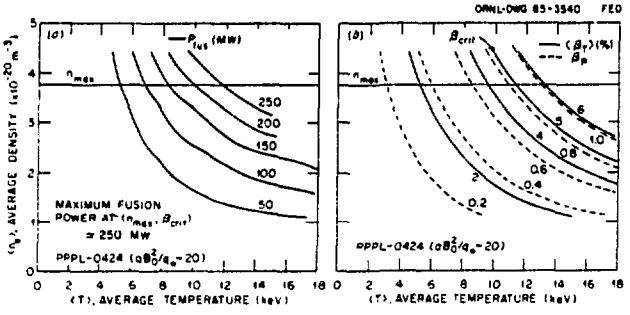


Fig. 9. POPCON plots for $aB_0^2/q_* \sim 20$ (PPPL) showing (a) steady-state thermal fusion power contours and (b) toroidal and poloidal beta contours (including fast-alpha pressure). (For stability, $\langle \beta_T \rangle < \beta_{crit} \sim 5\%$.)

Figs. 10-11. POPCON plots similar to those in Figs. 8-9 are given in Figs. 12-13. For this class of devices, ignition appears possible with some margin, even in the case of an L-mode scaling in a standard geometry (requiring $P_{aux} \sim$ 10-12 MW).

## 5. Conclusion

The results from both 0-D (analytic) and 1-1/2-D models indicate that there are classes of devices that appear ignitable with a finite operating window even under modestly conservative confinement scaling assumptions (such as L-mode of Kaye-Goldston). One such class consists of devices with $aB_0^2/q_* \sim$ 25-30, $\kappa \sim$ 1.8-2.0, $\delta \sim$ 0.2, $q_\psi \sim$ 2.6, and $A \sim$ 2.5-3.0, which offers a compromise between the examples considered in Sect. 4. From a purely physics point of view, a plausible set of device parameters may be $a \sim 0.5$ m, $R \sim 1.4$ m, $B_0 \sim$ 10-11 T, and $I \sim$ 10-11 MA. Detailed physics (burn dynamics, startup, volt-second requirements, MHD and sawtooth activities, etc.) and engineering design considerations will lead to further refinement of these parameters.


## Acknowledgment

Valuable discussions with H. P. Furth, PPPL, in formulating the ohmic + auxiliary scaling (Sect. 3.2) are greatly appreciated.


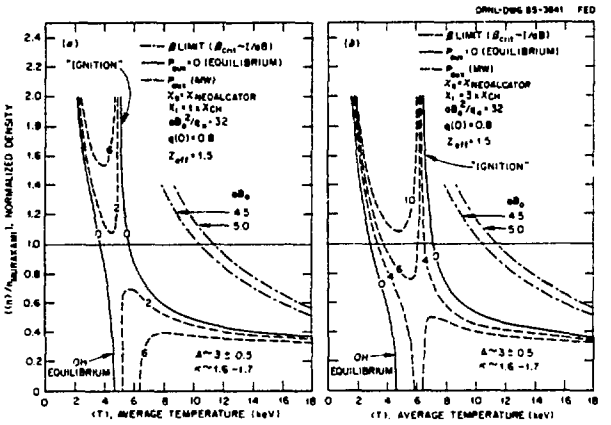


Fig. 10. Same as Fig. 6, except for classes of devices with $aB_0^2q_* \sim 32$.

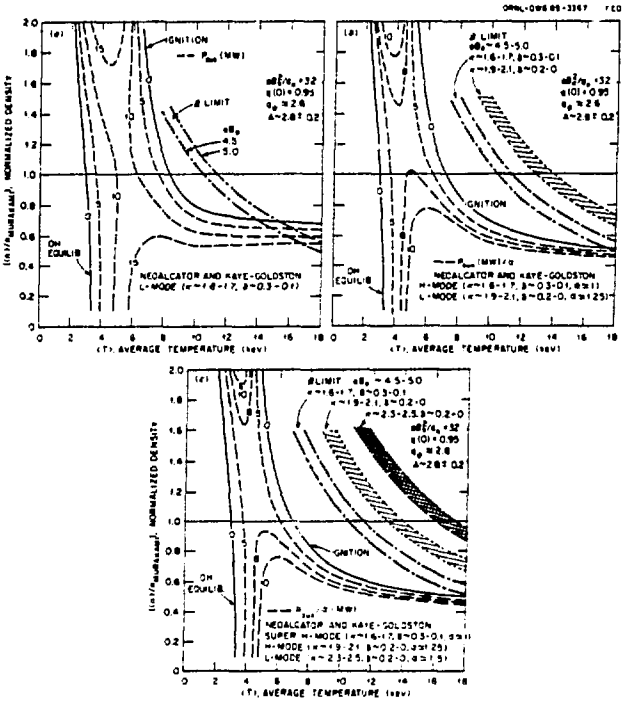


Fig. 11. Same as Fig. 7, except for classes of devices with $aB_0^2/q_* \sim 32$.

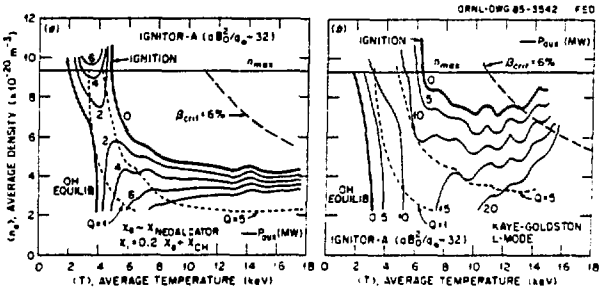


Fig. 12. Same as Fig. 8, except POPCON plots are for Ignitor-A ($n_{max} \sim 9.3 \times 10^{20}$ m$^{-3}$, $\beta_{crit} \sim 6\%$).

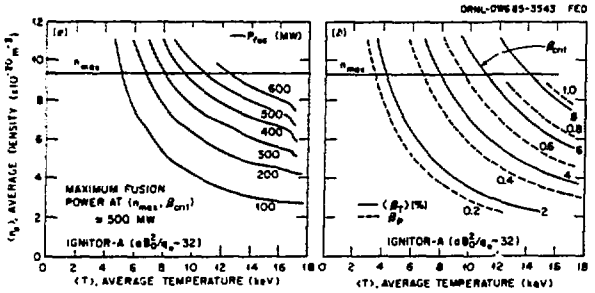


Fig. 13. Same as Fig. 9, except POPCON plots are for Ignitor-A. (For stability, $\langle\beta_T\rangle < \beta_{crit} \sim 6\%$.)

## Appendix: Global Power Balance Equation[2]

For simplicity, assuming profiles of the form $X = X_0(1 - \rho^2/a^2)^{\alpha_X}$, $X = n$, $T$, $J$, with $\alpha_n \sim 0.5$, $\alpha_T \sim 1.0$, and $\alpha_J = 3\alpha_T/2 \sim 1.5$, and taking $Z_{eff} \sim 1.5$ (with $Z \sim 8$ and $n_\alpha/n_e \sim 0.05$), the expressions for various powers (in MW/m$^3$) in Eq. (8) are as follows:

$$P_{con} = 0.16 n_{e20} T_{e10} (X_e + f_{nT} X_i) \left[\frac{4}{a^2}\left(\frac{1 + \kappa_*^2}{2\kappa^2}\right) g_1\right] \quad \text{(A-1a)}$$

$$= 0.24 n_{e20} T_{e10} \left(\frac{1}{\tau_{Ee}} + \frac{f_{nT}}{\tau_{Ei}}\right) g_2 \quad \text{(A-1b)}$$

$$= 0.24 n_{e20} T_{e10} [(1 + f_{nT})/\tau_E] g_2 \quad \text{(A-1c)}$$

$$P_{rad} = P_B \simeq 2.53 \times 10^{-2} (Z_{eff}/1.5) n_{e20}^2 T_{e10}^{1/2} \quad \text{(A-2)}$$

$$P_\alpha \simeq 0.22 (f_{nT}/0.9)^2 n_{e20}^2 T_{e10}^S \quad \text{(A-3)}$$

$$P_{OH} \simeq 2 \times 10^{-3} \left(\frac{Z_{eff}}{1.5}\right) \left(\frac{\bar{\gamma}_{NC}}{2.5}\right) T_{e10}^{-3/2} \left(\frac{B_0^2}{q_0^2 R_0^2}\right) \left(\frac{1 + \kappa_*^2}{2\kappa}\right)^2 , \quad \text{(A-4)}$$

where $f_{nT} = (n_i/n_e)(T_i/T_e) \sim 0.9$-$1.0$, $\kappa_*^2 \simeq \kappa^2(1 + 2\delta^2)$, $\bar{\gamma}_{NC}$ is the average (averaged over the temperature profile) neoclassical resistivity enhancement factor ($\bar{\gamma}_{NC} \simeq 2.5 \pm 0.3$ for $A = R_0/a \simeq 3.0 \mp 0.5$), $s \simeq 3$ (2) for $4 < T < 10$ keV ($10 < T < 20$ keV), and $g_1$ and $g_2$ are form factors determined from the profiles and the radius at which the temperature gradients are evaluated. (For the assumed profiles, taking gradients at $\rho/a \sim 0.7$-$0.8$, $g_1 \sim 1$-$1.3$ and $g_2 \sim 0.8$-$1.1$.) For the auxiliary power, radio-frequency-like heating with a Gaussian heating profile is assumed.

Using Eqs. (A-1)-(A-4) in Eq. (9) and defining a normalized density $m = n_{e20} R_0 q_*/(1.5\, B_0)$, the steady-state power balance equation ($F = -P_{con} - P_{rad} + P_\alpha + P_{OH} + P_{aux} = 0$) may be written as

$$-f_{con}(m, T) - a_B m^2 T_{10}^{1/2} + a_\alpha m^2 T_{10}^S + a_{OH} T_{10}^{-3/2} + a_{aux} = 0 , \quad \text{(A-5)}$$

where

$$f_{con}(m, T_{10}) \simeq 1.8 m^2 T_{10} \left(\frac{X_e}{n_{e20} a^2} + f_{nT} \frac{X_i}{n_{e20} a^2}\right) \left(\frac{1 + \kappa_*^2}{2\kappa^2}\right)$$

$$\simeq 0.54 m^2 T_{10} (1 + f_{nT})/(n_{e20} \tau_E) , \quad \text{(A-6)}$$

$$a_B \simeq 5.7 \times 10^{-2} (Z_{eff}/1.5) , \quad \text{(A-7a)}$$

$$a_\alpha \simeq 0.5 (f_{nT}/0.9)^2 , \quad \text{(A-7b)}$$

$$a_{OH} \simeq 2 \times 10^{-3} (q_*^2/q_0^2)(\bar{\gamma}_{NC}/2.5)(Z_{eff}/1.5)[(1 + \kappa_*^2)/2\kappa]^2 , \quad \text{(A-7c)}$$

$$a_{aux} = (P_{aux}/2\pi^2)(R_0 q_*/a\kappa)/(aB_0^2/q_*) . \quad \text{(A-7d)}$$

[Note that $q_*(a)/q(0) = q_*/q_0 = 1 + \alpha_J = 1 + 3\alpha_T/2$.]

In steady state ($F = 0$), the ignition condition is $P_{con} + P_{rad} = P_\alpha + P_{OH}$. At low enough temperatures, this condition can also be satisfied, corresponding to ohmic (OH) equilibrium.

Thermal runaway is defined by $F = \partial F/\partial T = \partial P_{aux}/\partial T = 0$, which is satisfied at $T = T_*$, where $P_{aux} = P_{aux}(max)$ along a line of constant density.

The optimal path to ignition (saddle point) is determined from $F = \partial F/\partial T = \partial F/\partial n = 0$, which is satisfied at $(n_*, T_*)$ where $P_{aux}(max)$ is minimum. If $P_{aux} = 0$, this gives the optimal condition for ohmic ignition ($F = P_{aux} = \partial F/\partial T = \partial F/\partial n = 0$). For an energy confinement time of the form $\tau_E \sim n^X T^y$, the optimal path (saddle point) can be determined from

$$[(1 + x)/2] P_{con} = P_{aux} + P_{OH} ,$$

$$[(1 - x)/2] P_{con} = P_\alpha - P_{rad} , \quad \text{(A-8)}$$

$$2(1 - y) P_{con} = 2sP_\alpha - 3P_{OH} - P_{rad} .$$

If $P_{aux} = 0$, Eq. (A-8) gives the *minimum* condition for ohmic ignition. For example, considering $\tau_{Ee} \sim \tau_{NA}(x = 1, y = 0)$ and $\tau_{Ei} \sim \tau_{iCH}(x = -1, y = 1/2)$ we have (for $s = 3$) $P_\alpha = P_i + P_{rad} = P_e - 0.6P_{aux} = P_{OH} + 0.4P_{aux}$ at the saddle point, from which the minimum $P_{aux}$ can be calculated. [The OH ignition condition for this case is $P_\alpha = P_i + P_{rad} = P_e = P_{OH}$.]

## References


1. B. Coppi, "Compact experiments for α-particle heating," Comments Plasma Phys. Controlled Fusion, vol. 3, pp. 47-62, 1977.
2. N. A. Uckan and J. Sheffield, "A simple procedure for establishing ignition conditions in tokamaks," in Tokamak Startup - Problems and Scenarios Related to the Transient Phases of Tokamak Operation (Erice School of Tokamak Startup, 1985; proceedings to be published); Oak Ridge National Laboratory Report ORNL/TM-9722 (1985); and N. A. Uckan, J. Sheffield, and E. C. Selcow, "A simple contour analysis of ignition conditions and plasma operating regimes in tokamaks," these proceedings.
3. W. A. Houlberg, S. E. Attenberger, and L. M. Hively, "Contour analysis of fusion reactor plasma performance," Nucl. Fusion, vol. 22, pp. 935-945, 1982.
4. B. Coppi, "Nonclassical transport and the principle of profile consistency," Comments Plasma Phys. Controlled Fusion, vol. 5, pp. 261-269, 1980.
5. S. M. Kaye et al., "Thermal energy confinement scaling in PDX limiter discharges," Nucl. Fusion, vol. 24, pp. 1303-1334, 1984.
6. M. Murakami et al., "Confinement studies of neutral beam heated discharges in TFTR," in Proc. 12th European Conf. on Controlled Fusion and Plasma Phys. (Budapest, Hungary, Sept. 2-6, 1985).
7. W. A. Houlberg, "Plasma engineering assessment of compact ignition experiments," these proceedings.
8. M. Murakami et al., "Some observations on maximum densities in tokamak experiments," Nucl. Fusion, vol. 16, pp. 347-348, 1976.
9. F. Troyon et al., "MHD limits to tokamak confinement," Plasma Phys. Controlled Fusion, vol. 26, pp. 209-215, 1984.

10. C. S. Chang and F. L. Hinton, "Effect of finite aspect ratio on the neoclassical thermal conductivity in the banana regime," Phys. Fluids, vol. 25, pp. 1493-1494, 1982.
11. S. M. Kaye, "A review of energy confinement and local transport scaling results in neutral-beam heated tokamaks," Phys. Fluids, vol. 28, pp. 2327-2343, 1985.
12. R. J. Goldston, "Energy confinement scaling in tokamaks: some implications of recent experiments with ohmic and strong auxiliary heating," Plasma Phys. Controlled Fusion, Vol. 26, pp. 87-103, 1984.
13. H. P. Furth, private communication, 1985.
14. B. Coppi, "An advanced burning core experiment," MIT R.L.E. Report PTP-84/17 (1984).
15. J. A. Schmidt et al., PPPL Ignition studies, private communication, 1984-1985.
16. D. R. Cohn et al., MIT LITE studies, private communication, 1984-1985.

## DISCLAIMER